LAWRENCE
LIVERMORE
NATIONAL
LABORATORY

LLNL-JRNL-645206

Persistent Fe moments in the normal state of the pressure-induced superconductor Ca0.67Sr0.33Fe2As2

J. R. Jeffries, N. P. Butch, M. J. Lipp, J. A. Bradley, K. Kirshenbaum, S. R. Saha, J. Paglione, C. Kenney-Benson, Y. Xiao, P. Chow, W. J. Evans

October 24, 2013

Physical Review B

Disclaimer

Persistent Fe moments in the normal state of the pressure-induced superconductor $Ca_{0.67}Sr_{0.33}Fe_2As_2$

J. R. Jeffries,[1] N. P. Butch,[1] M. J. Lipp,[1] J. A. Bradley,[1] K. Kirshenbaum,[2] S. R. Saha,[2] J. Paglione,[2] C. Kenney-Benson,[3] Y. Xiao,[3] P. Chow,[3] and W. J. Evans[1]

[1] *Condensed Matter and Materials Division, Lawrence Livermore National Laboratory, Livermore, CA 94550, USA*
[2] *Center for Nanophysics and Advanced Materials, Department of Physics, University of Maryland, College Park, MD 20742, USA*
[3] *HP-CAT, Geophysical Laboratory, Carnegie Institute of Washington, Argonne, IL 60439, USA*

(Dated: October 21, 2013)

Using non-resonant Fe $K\beta$ x-ray emission spectroscopy, we reveal that the Fe moments of $Ca_{0.67}Sr_{0.33}Fe_2As_2$ persist into the pressure-induced collapsed tetragonal phase, yielding a paramagnetic normal state out of which superconductivity develops. While the persistent moment is in contrast to that of undoped $CaFe_2As_2$, x-ray diffraction measurements implicate the c-axis lattice parameter as the controlling criterion for the Fe moment. These results evoke a general description for the behavior of the alkaline-earth based 122 systems under pressure that lends support to theories for superconductivity involving unconventional pairing mediated by magnetic fluctuations.

PACS numbers: 74.70.Xa, 75.20.Hr, 64.70.Kd, 78.70.En

Early in the research on the iron pnictide superconductors, theoretical calculations strongly suggested that conventional, phonon-mediated superconductivity was incompatible with observed critical temperatures T_c [1–4]. Additionally, several systems have shown an empirical correlation between T_c and the structural parameters [5–7]. Since then, iron-based superconductors have proven a fertile playground for understanding how structural and magnetic degrees of freedom affect superconductivity [8–11]. While there are no fewer than five systems sharing similar structural building blocks, the most widely studied ferropnictide superconductors are those that crystallize in the tetragonal $ThCr_2Si_2$ crystal structure. The so-named "122" compounds have the chemical formula AFe_2X_2 (where A is an alkaline-earth element, an alkali metal, or Eu and X is a pnictogen atom), exhibit antiferromagnetic order at ambient pressure, and are amenable to a variety of chemical substitutions that suppress magnetism and induce superconductivity[8, 9, 11–14].

With applied pressure or suitable chemical substitution, the parent 122 compounds undergo an isostructural volume collapse that is driven by the development of As-As bonding [15–19]. This collapsed tetragonal (CT) phase abruptly cuts off the antiferromagnetic order and, in most cases, supports superconductivity in the vicinity of the truncated magnetic order. The dissenting member of the 122 family, $CaFe_2As_2$, shows no signs of superconductivity in the CT phase when subjected to hydrostatic compression or isovalent P substitution, which mimics pressure through a reduction in the unit cell volume [20, 21]. This absence of superconductivity resonates with scenario where the Fe moments in the CT phase of $CaFe_2As_2$ are quenched [22], supporting the strong link between the presence of magnetic fluctuations and the occurrence of superconductivity in this family of compounds [3, 4]. However, in Pr- and Nd-doped $CaFe_2As_2$, superconductivity can be induced from a normal state comprising non-magnetic Fe atoms [23]. These opposing behaviors with respect to the magnetic state of the Fe atoms call question the roles of magnetic and charge fluctuations in inducing superconductivity in the 122 systems.

In order to tune the structural and magnetic degrees of freedom without charge doping, we have performed high-pressure experiments on $Ca_{0.67}Sr_{0.33}Fe_2As_2$, which provides larger-volume system (relative to $CaFe_2As_2$) that permits access to a broader range of structural parameters. In this Letter, using non-resonant Fe $K\beta$ x-ray emission spectroscopy (XES) and x-ray diffraction (XRD), we report the evolution of the instantaneous Fe moments of $Ca_{0.67}Sr_{0.33}Fe_2As_2$ as a function of pressure and crystal structure. We find that the Fe moments persist into the CT phase, providing a magnetic normal state out of which superconductivity develops. The presence of Fe moments, or lack thereof, appears to be largely controlled by structural parameters.

Single crystals of $(Ca_{0.67}Sr_{0.33})Fe_2As_2$ were synthesized with a flux-growth technique previously described [24]. For the XES measurements, small single crystals were loaded into diamond anvil cells (DAC) that employed Be gaskets (∼3 mm diameter), while, for XRD experiments, a powder was loaded into a spring steel gasket. The DAC was pressurized using a gas membrane, and the pressure in the sample chamber was calibrated using the shift of the ruby fluorescence line (XES data) or the lattice parameter of Cu (XRD data). Silicone oil (XES data) or neon (XRD data) were used as the pressure-transmitting media.

The XES measurements were performed at beamline 16-IDD and the XRD measurements at 16-BMD of the High-Pressure Collaborative Access Team (HP-CAT) at the Advanced Photon Source. For XES, 11.3-

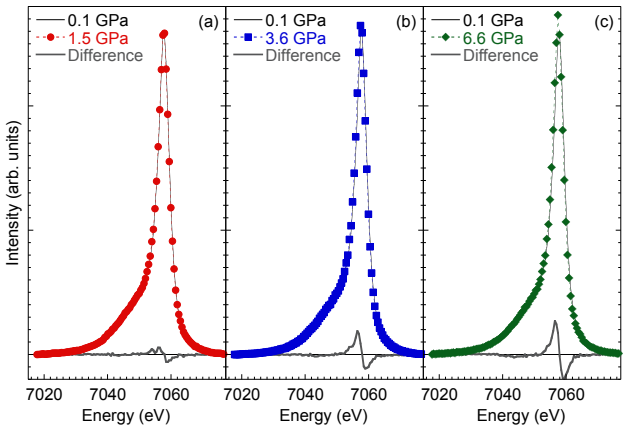

FIG. 1: (color online) Room-temperature XES spectra of $(Ca_{0.67}Sr_{0.33})Fe_2As_2$ under pressure (dashed lines, closed symbols) at 1.5 (a), 3.6 (b), and 6.6 (c) GPa as compared the spectrum at 0.1 GPa (black line, no symbols). The differences between the XES data at each pressure and those at 0.1 GPa are shown as the grey solid lines below the data.

and 20.0-keV, micro-focused x-ray beams (approximately 80x80 μm^2) entered through one of the diamond anvils, while the emitted Fe $K\beta$ x-rays were collected after passing through the Be gasket. Fe $K\beta$ spectra were acquired by scanning a bent Si (333) analyzer in 0.25 eV steps; resolution was 1 eV. XRD data were collected in a transmission geometry using a 30 keV, 10x10 μm^2 micro-focused x-ray beam and a Mar345 Image plate. Analysis procedures for the XRD data are identical to Ref. 18. Additionally, for the 20.0 keV incident energy XES setup, x-ray diffraction was performed *in situ* to confirm the crystal structure of the $Ca_{0.67}Sr_{0.33}Fe_2As_2$ specimen. Low-temperature XES and XRD measurements were performed in a He-flow cryostat.

The Fe $K\beta$ spectra are sensitive, bulk probes of the instantaneous Fe moment due to atomic $3p$-$3d$ orbital overlap. An incoming x-ray with an energy greater than the Fe K-edge can excite a $1s$ electron from the core of an Fe atom into the continuum, leaving a $1s$ core-hole that can be filled with a decay from the $3p$ shell. This $3p-1s$ decay in Fe emits an x-ray, the $K\beta$ line, at 7058 eV and leaves a final-state core-hole in the $3p$ level. In the presence of a $3d$ moment, the spin degeneracy of this $3p$ core-hole is lifted, producing an energy difference between the spin states of the $3p$ core-hole, and yielding an emission spectrum with a predominant $K\beta$ peak and a weaker satellite $K\beta'$ peak [25]. For small-moment systems, like $Ca_{0.67}Sr_{0.33}Fe_2As_2$, the $K\beta'$ portion of a spectrum appears as a shoulder, rather than a distinct peak, on the low-energy side of the main $K\beta$ peak. Unfortunately, a low-energy shoulder exists even in non-magnetic Fe systems, and, as such, a systematic analysis of the *entire* emission spectrum is necessary to extract a quantitative Fe moment. Here we follow the integrated absolute difference (IAD) method to evaluate the Fe moment in $Ca_{0.67}Sr_{0.33}Fe_2As_2$ under pressure [26]. An IAD analysis proceeds as follows: each spectra is normalized such that its integral is unity, a unit-normalized reference spectrum is subtracted from each spectra to yield a difference spectra, and the absolute values of the difference spectra are integrated to yield a quantitative IAD value that is proportional to the Fe moment for each spectra. For tetrahedrally coordinated Fe atoms, the IAD value can be converted to an Fe moment (in μ_B) using the calibration provided by Gretarsson, *et al* [27]. Here, we use our room-temperature, 0.1-GPa data as the reference; Fe moment measurements are thus measured relative to that at 0.1 GPa, which is near enough to ambient pressure to use the ambient-pressure value of about 1.1 μ_B for the $AEFe_2As_2$ systems[27].

Example room-temperature XES measurements are shown in Figures 1a-c, which display the unit-normalized Fe $K\beta$ spectra at 1.5, 3.6, and 6.6 GPa as compared to the spectrum at 0.1 GPa. The shoulder associated with the $K\beta'$ satellite is clearly evident in the low-energy asymmetry of the main peak. The differences between the reference spectrum (0.1-GPa data) and the high-pressure spectra are shown as the solid, grey lines. With increasing pressure, the difference spectra clearly grow larger. The negative dip seen at 6.6 GPa near 7045 eV indicates a loss of spectral weight in the $K\beta'$ satellite portion of the spectrum, implying a reduction in the Fe moment with increasing pressure.

The IAD values from each pressure at 300 and 125 K have been converted to Fe moments, and these values are shown in Fig. 2a. At both 125 and 300 K, pressure drives the Fe moment down linearly; the slope of the pressure dependence of the Fe moment, -0.15 μ_B/GPa, is identical within our experimental precision for both temperatures. The measured isotherms are overlaid on the phase diagram shown in Fig. 2b. At 300 K, the structure of $(Ca_{0.67}Sr_{0.33})Fe_2As_2$ undergoes a tetragonal (T) to collapsed-tetragonal (CT) phase transition near 4 GPa [18]. At 125 K and ambient pressure, $(Ca_{0.67}Sr_{0.33})Fe_2As_2$ is antiferromagnetically ordered (AFM), and the crystal structure is orthorhombic (O) rather than tetragonal. With pressure at 125 K, the system undergoes an O-T transformation that destroys AFM order in favor of a paramagnetic (PM) state at about 2 GPa; the T-CT phase transition occurs near 2.8 GPa. The Fe moment evolves relatively smoothly through each of these structural/magnetic phase transitions.

In addition to the phase boundaries of Fig. 2b, a contour plot of the Fe moment in T-P space is included. A linear interpolation is employed between 300 and 125 K, and the same trend is extrapolated to lower temperatures. This linear extrapolation seems reasonable given the nearly linear temperature dependence (for

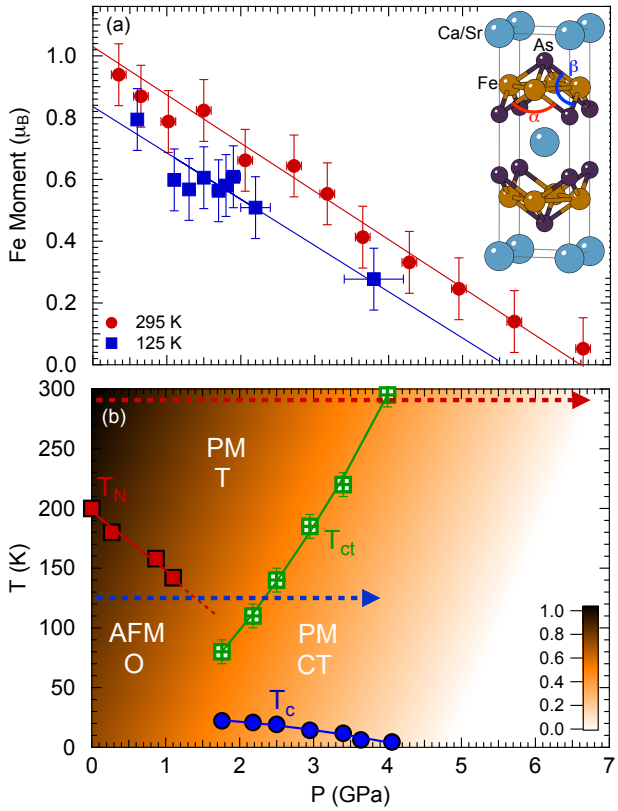

FIG. 2: (color online) (a) The pressure-dependent Fe moment of $(Ca_{0.67}Sr_{0.33})Fe_2As_2$ at 295 and 125 K; solid lines through the data are linear fits. Horizontal error bars are the larger of 0.1 GPa or the difference between the pressures before and after collection of the spectra. Vertical error bars are 0.1 μ_B estimated from the noise in the spectra. The inset displays the crystal structure of $(Ca_{0.67}Sr_{0.33})Fe_2As_2$, and labels the two As-Fe-As bond angles. (b) The electronic and structural phase diagram of $(Ca_{0.67}Sr_{0.33})Fe_2As_2$ [18], including a contour plot of the Fe moment in μ_B. The arrows indicate the approximate paths of the XES measurements.

$T \gtrsim 50$ K) of the moment and lattice parameters of $(Ca_{0.78}La_{0.22})Fe_2As_2$ [23]. At 1.8 GPa, this extrapolation implies a moment of 0.4 μ_B at 25 K, just above the value of $T_c \approx 22$ K. The suppression of superconductivity with pressure follows that of the Fe moment, with T_c disappearing very close to the pressure at which the Fe moment goes to zero. These observations suggests that the superconducting state of $(Ca_{0.67}Sr_{0.33})Fe_2As_2$ not only develops out of a magnetic normal state, but also that T_c is correlated with the magnitude of the Fe moment. The persistent moment near T_c is in contrast to that seen in Pr- and Nd-doped $CaFe_2As_2$, but it is comparable to $(Ca_{0.78}La_{0.22})Fe_2As_2$, where an approximately 0.5 μ_B moment is present with $T_c \approx 35$ K [19, 23]. Finally, the persistence of the Fe moment into the CT phase implies that the AFM phase is destroyed by means other than quenching of the local moments. Rather, a more favorable scenario would likely be one where the CT phase supports enhanced spin fluctuations or alters coupling strengths that lead to the destruction of magnetic order [10]

Unlike the temperature dependent moments of Pr- and Nd-doped $CaFe_2As_2$ [23], the Fe moments at 300 and 125 K (Fig. 2a) of $(Ca_{0.67}Sr_{0.33})Fe_2As_2$ do not exhibit any large discontinuities upon crossing the T-CT or O-T phase boundaries. While this may at first appear inconsistent, a closer examination of the effect of structure on the Fe moments reveals common behavior. Figure 3 shows the evolutions of the following structural parameters of $(Ca_{0.67}Sr_{0.33})Fe_2As_2$ at 300 and 125 K as functions of the Fe moment: the orthorhombic (a_O and b_O)

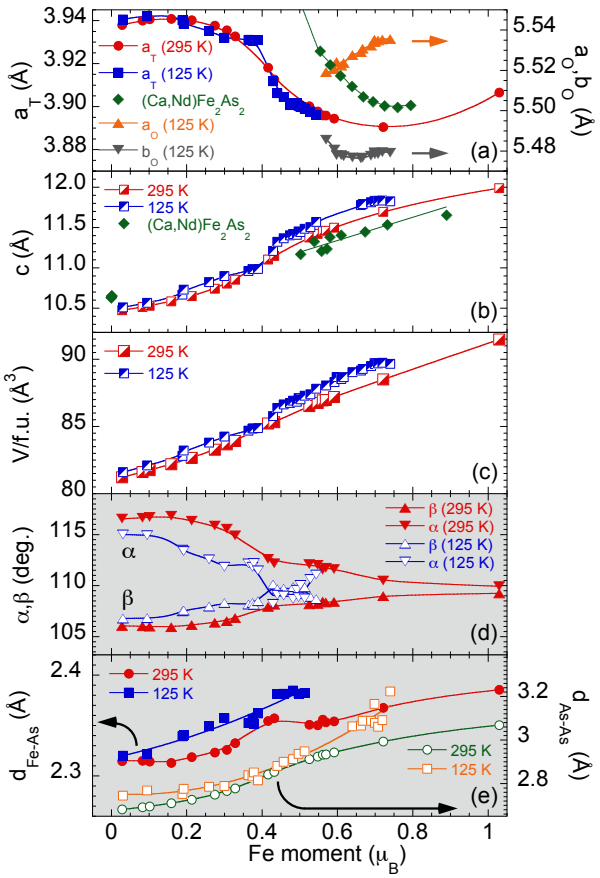

FIG. 3: (color online) Crystal structure parameters of $(Ca_{0.67}Sr_{0.33})Fe_2As_2$ as a function of Fe moment for different temperatures: (a) a_T, a_O, and b_O, lattice parameters; (b) c lattice parameter; and (c) unit cell volume per formula unit V.f.u. The internal degrees of freedom of the crystal structure: (d) As-Fe-As bond angles (see inset of Fig. 2), and (e) the Fe-As and As-As bond distances. The a- and c-axis lattice parameters (from temperature-dependent measurements) for $(Ca_{0.92}Nd_{0.08})Fe_2As_2$ are included in (a) and (b), respectively [23].

and tetragonal (a_T) basal plane lattice parameters; the c-axis lattice parameter; the volume per formula unit ($V/f.u.$); the As-Fe-As bond angles; as well as the Fe-As bond length (d_{Fe-As}) and the As-As mirror plane spacing (d_{As-As}). The a_T, c, and V/f.u. parameters show significant overlap at 300 and 125 K, whereas the Fe-As separation and the As-Fe-As bond angles do not. This implies that the lattice parameters, rather than the internal structural degrees of freedom, are the dominant factors controlling the magnitude of the Fe moment in $(Ca_{0.67}Sr_{0.33})Fe_2As_2$.

Including data from $(Ca_{0.92}Nd_{0.08})Fe_2As_2$ further illuminates the correlations between structure and Fe moment. Figs. 3(a) and (b) include structure data for $(Ca_{0.92}Nd_{0.08})Fe_2As_2$ taken as a function of temperature [19, 23]. While the T-dependent (and thus Fe-moment-dependent) a-axis lattice parameter of Nd-doped $CaFe_2As_2$ is distinctly different from that of $(Ca_{0.67}Sr_{0.33})Fe_2As_2$ under pressure, the c-axis lattice parameters for these compounds follow strikingly similar behavior as a function of Fe moment. The temperature-induced T-CT transition in $(Ca_{0.92}Nd_{0.08})Fe_2As_2$ results in a large ($\sim$5%) change in the c-axis lattice parameter that yields a zero-moment CT phase with c <10.65 Å [23]. When the c-axis lattice parameter of $(Ca_{0.67}Sr_{0.33})Fe_2As_2$ is compressed to the same value c <10.65 Å at either 300 or 125 K, the Fe moment is similarly lost. The strong correlation between c-axis lattice parameter and the Fe moment is in excellent qualitative agreement with theoretical calculations [3, 10].

These experimental results challenge the notion that the Fe moment is universally quenched in the CT phase of the 122 systems. While the Fe moments in the CT phase of undoped $CaFe_2As_2$ are quenched [22], we have shown that the CT phase can in fact support a substantial Fe moment ($\sim$0.4 μ_B) that is strongly coupled to the c-axis lattice parameter of the system. The persistence of an Fe moment into the CT phase provides a paramagnetic normal state out of which superconductivity can develop even in the absence of charge doping. Furthermore, the pressure-dependent suppression of T_c tracks that of the Fe moment, with T_c approaching zero within approximately 0.5 GPa of the pressure at which the Fe moment would be expected to quench at very low temperature. These observations support the picture of an unconventional superconducting state mediated by magnetic fluctuations.

We are grateful to K. Visbeck for assistance with cell preparations. Portions of this work were performed under LDRD (11-LW-003). Lawrence Livermore National Laboratory is operated by Lawrence Livermore National Security, LLC, for the U.S. Department of Energy, National Nuclear Security Administration under Contract DE-AC52-07NA27344. Portions of this work were performed at HPCAT (Sector 16), Advanced Photon Source (APS), Argonne National Laboratory. HPCAT operations are supported by DOE-NNSA under Award No. DE-NA0001974 and DOE-BES under Award No. DE-FG02-99ER45775, with partial instrumentation funding by NSF. APS is supported by DOE-BES, under Contract No. DE-AC02-06CH11357. Beamtime was provided through the Carnegie-DOE Alliance Center (CDAC) and the APS General User Program (GUP). This work was partially supported by AFOSR-MURI Grant No. FA9550-09-1-0603.

[1] L. Boeri, O. V. Dolgov, and A. A. Golubov, Phys. Rev. Lett. **101**, 026403 (2008).
[2] I. I. Mazin, D. J. Singh, M. D. Johannes, and M. H. Du, Phys. Rev. Lett. **101**, 057003 (2008).
[3] T. Yildirim, Phys. Rev. Lett. **102**, 037003 (2009).
[4] P. J. Hirschfeld, M. M. Korshunov, and I. I .Mazin, Rep. Prog. Phys. **74**, 124508 (2011).
[5] C. -H. Lee, *et al.*, J. Phys. Soc. Jpn. **77**, 083704 (2008).
[6] J. Zhao, *et al.*, Nat. Mater. **7**, 953 (2008).
[7] S. A. J. Kimber, *et al.*, Nat. Mater. **8**, 471 (2009).
[8] J. Paglione and R. L. Greene, Nat. Phys. **6**, 645 (2010).
[9] D. C. Johnston, Adv. Phys. **59**, 803 (2010).
[10] M. D. Johannes, I. I. Mazin, and D. S. Parker, Phys. Rev. B **82**, 024527 (2010).
[11] G. R. Stewart, Rev. Mod. Phys. **83**, 1589 (2011).
[12] M. D. Lumsden and A. D. Christianson, J. Phys.: Condens. Matter **22**, 203203 (2010).
[13] M. Gooch, B. Lv, K. Sasmal, J. H. Tapp, A. J. Tang, A. M. Guloy, B. Lorenz, and C. W. Chu, Physica C **470**, S276 (2010).
[14] H. S. Jeevan, Z. Hossain, D. Kasinathan, H. Rosner, C. Geibel, and P. Gegenwart, Phys. Rev. B **78**, 052502 (2008).
[15] A. I. Goldman, A. Kreyssig, K. Prokeš, D. K. Pratt, D. N. Argyriou, J. W. Lynn, S. Nandi, S. A. J. Kimber, Y. Chen, Y. B. Lee, G. Samolyuk, J. B. Leão, S. J. Poulton, S. L. Bud'ko, N. Ni, P. C. Canfield, B. N. Harmon, and R. J. McQueeney, Phys. Rev. B **79**, 024513 (2009).
[16] W. O. Uhoya, J. M. Montgomery, G. M. Tsoi, Y. K. Vohra, M. A. McGuire, A. S. Sefat, B. C. Sales, and S. T. Weir, J. Phys.: Condens. Matt. **23**, 122201 (2011).
[17] R. Mittal, S. K. Mishra, S. L. Chaplot, S. V. Ovsyannikov, E. Greenberg, D. M. Trots, L. Dubrovinsky, Y. Su, T. Brueckel, S. Matsuishi, H. Hosono, G. Garbarino, Phys. Rev. B **83**, 054503 (2011).
[18] J. R. Jeffries, N. P. Butch, K. Kirshenbaum, S. R. Saha, G. Samudrala, S. T. Weir, Y. K. Vohra, and J. Paglione, Phys. Rev. B **85**, 184501 (2012).
[19] S. R. Saha, N. P. Butch, T. Drye, J. Magill, S. Ziemak , K. Kirshenbaum, P. Y. Zavalij, J. W. Lynn, and J. Paglione, Phys. Rev. B **85**, 024525 (2012).
[20] W. Yu, A. A. Aczel, T. J. Williams, S. L. Budko, N. Ni, P. C. Canfield, and G. M. Luke, Phys. Rev. B **79**, 020511(R) (2009).
[21] S. Kasahara, T. Shibauchi, K. Hashimoto, Y. Nakai, H. Ikeda, T. Terashima, and Y. Matsuda, Phys. Rev. B **83**, 060505(R) (2011).
[22] A. Kreyssig, *et al.*, Phys. Rev. B **78**, 184517 (2008).
[23] H. Gretarsson, S. R. Saha, T. Drye, J. Paglione, J. Kim,

D. Casa, T. Gog, W. Wu, S. R. Julian, and Y. -J. Kim, Phys. Rev. Lett. **110**, 047003 (2013).
[24] S. R. Saha, N. P. Butch, K. Kirshenbaum, J. Paglione, and P. Y. Zavalij, Phys. Rev. Lett. **103**, 037005 (2009).
[25] J. -F. Lin, V. V. Struzhkin, S. D. Jacobsen, M. Y. Hu, P. Chow, J. Kung, H. Liu, H. -K. Mao, and R. J. Hemley, Nature **436**, 377 (2005).
[26] G. Vankó, T. Neisius, G. Molnár, F. Renz, S. Kárpáti, A. Shukla, F. M. F. de Groot, J. Phys. Chem B **110**, 11647 (2006).
[27] H. Gretarsson, *et al.*, Phys. Rev. B **84**, 100509(R) (2011).